

Region resolvability versus noise level characteristics for joint spatial and kinetic parameter estimation in inconsistent projection dynamic ECT ¹

JS Maltz, *Member, IEEE*

Center for Functional Imaging, Lawrence Berkeley National Laboratory and
Department of Electrical Engineering and Computer Science, University of California at Berkeley

Abstract

For emission computed tomography (ECT) studies of temporally static source distributions, well-known guidelines exist for the number of resolution elements which may be acceptably resolved in a reconstructed image, at a given noise level. Owing to the incomplete angular-temporal sampling in such ECT modalities as rotating camera dynamic single photon ECT (SPECT), the acquired sinogram is not a consistent representation of a Radon transform, and consequently, no analogous bounds on the performance of dynamic reconstruction algorithms may be derived from Radon transform theory. Applying what we believe to be the first spatiokinetic parameter estimation algorithm able to simultaneously estimate both the geometry and kinetics of multiple dynamic regions directly from inconsistent projections, we establish empirical estimates for the number of regions whose boundaries and time-activity curves (TAC's) may be simultaneously estimated to a specified degree of accuracy at a given signal-to-noise ratio (SNR). Surprisingly, we find that regional TAC recovery for a segmented annulus myocardial phantom is relatively insensitive to noise at realistic SNR's and to a twofold increase in the number of resolution elements. We conclude that errors in the recovered regional TAC's are due primarily to the poorly conditioned nature of the spatiokinetic parameter estimation problem.

I. INTRODUCTION

Resolution versus noise characteristics for static ECT imaging, where time-invariance of the radionuclide source distribution is assumed, are useful guidelines in the design of clinical studies. While well-developed Radon transform inversion theory equips us with the analytical tools to determine the limits on resolvability in the static case, the non-linear problem of simultaneously estimating both the underlying geometry and time-activity within a dynamic source distribution is far more difficult to analyze. This is due, in part, to the fact that resolvability is dependent on the source configuration, the number of the dynamic regions, and the nature of their time-activity evolution. In the case where a distribution is imaged using rotating cameras which cannot simultaneously measure all projections throughout the duration of the study, reconstruction without the assumption of a geometric and kinetic model for the regions is impossible. Single camera, single rotation acquisition, is equivalent to sampling the time-varying Radon transform along the plane

shown in Figure 1 (for a 2D slice). Reconstruction of the source distribution requires that the transform be sampled sufficiently on $\mathbb{R}^2 \times \mathbb{R}^1$ over the entire duration of the acquisition. The only way to determine the missing sample points is through interpolation, which requires both a region (or pixel) model, and models for the TAC's of each region. Consequently, resolvability estimates can only be derived under the assumption of such a model.

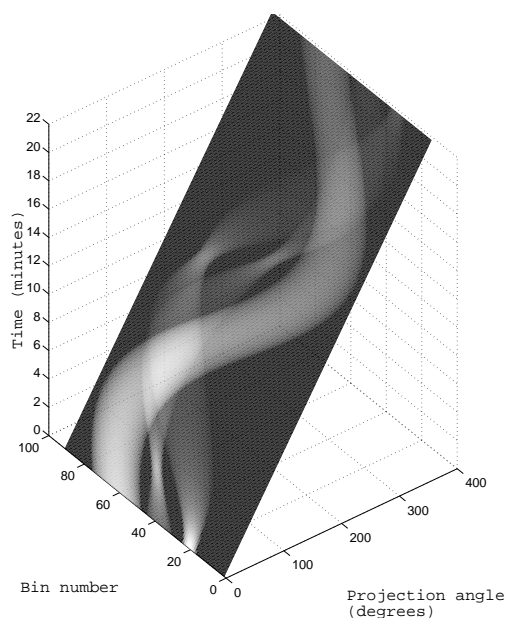


Figure 1: The sinotimogram, or sinogram of a time-varying distribution, illustrates the fact that single rotating camera imaging of dynamic sources is equivalent to sampling along a single plane in Radon-time space. Without a spatiotemporal model of the sources, interpolation in this space is impossible.

In [1], we formulated an algorithm for joint spatial and kinetic parameter estimation, which is a non-trivial extension of the single dynamic region method of Chiao et al. to the case where more than one dynamic region (model compartment) is present among the imaged sources [2]. This algorithm fits a multiple elliptical region model directly to measured projection data. The time activity within each ellipse is the sum of the responses of one or more single compartment models. This model is particularly suited to ^{99m}Tc-teboroxime myocardial studies. While it might fairly be argued that the ellipse is a suboptimal shape for the approximation of the source geometry, the fact that it has a simple analytic differentiable Radon transform renders it useful for the characterization of this problem. We also find in practice that the geometric approximation error is small in relation to other sources of error which contribute towards biases is the parameter estimates.

¹This work was supported by US Department of Health and Human Services grant HL-07367, by US Department of Energy contract DE-AC03-76SF00098 and by the South African National Research Foundation.

Here, we perform over 150 phantom data experiments using this method in order to establish how well the TAC's of dynamic regions may be recovered as the number of regions and the SNR changes. For the sake of convenience, we begin with a brief summary of the method presented in [1].

II. JOINT SPATIOTEMPORAL PARAMETER ESTIMATION FOR MULTIPLE DYNAMIC REGIONS

We begin by stating the core assumptions implicit in the development of this algorithm:

1. Each modeled region is homogeneous.
2. We ignore the effects of attenuation within the body. While this is a poor assumption in ECT, compensation may be effected using an attenuation map obtained through a transmission study.
3. The time-varying intensities of all dynamic regions within the distribution are characterized by first order tracer kinetics.
4. Region boundaries are static throughout the imaging process.
5. The blood input function is known.
6. Without loss of generality, we assume that all projection data are acquired using a single-headed camera, which performs a single rotation about the activity distribution during the imaging process.

A. Model description

We employ the ellipse as spatial modeling element since it possesses a simple and analytically differentiable Radon transform. In this way, the entire model sinogram is differentiable, allowing efficient employment of deterministic optimization algorithms for the maximization of the likelihood function.

A typical arrangement of such ellipses in the representation of a myocardium containing several dynamic regions appears in Figure 2.

The parameterized model sinogram which is fit directly to the acquired sinogram, consists of the projections of N ellipses $E_n(\mathbf{x}_n)$ centered at (u_n, v_n) with orientation Ω_n and respective semimajor and semiminor axes a_n and b_n

$$E_n(\mathbf{x}_n) = \left\{ (u, v) \mid a_n^{-2} (u \cos(\Omega_n) - v \sin(\Omega_n) - u_n)^2 + b_n^{-2} (u \sin(\Omega_n) + v \cos(\Omega_n) - v_n)^2 \leq 1 \right\}. \quad (1)$$

Each possesses a time-varying activity of the form:

$$I_n(t) = i(t) * \sum_{m=1}^M k_1^{mn} e^{-k_2^{mn} t}, \quad (2)$$

where $i(t)$ is the compartmental input function, and '*' denotes convolution. The vector \mathbf{x}_n contains the geometric and kinetic parameters for the n th shape, and is defined as

$$\mathbf{x}_n = (a_n, b_n, \alpha_n, k_1^{1n}, k_1^{2n}, \dots, k_1^{Mn}, k_2^{1n}, k_2^{2n}, \dots, k_2^{Mn}, u_n, v_n). \quad (3)$$

In order that we may restrict the orientation of one ellipse with respect to those of its neighbors using simple interval bounds, we parameterize the relative angle between successive ellipses as α_n such that:

$$\Omega_n = \sum_{i=1}^n \alpha_i.$$

This parameterization allows us to prevent the string of ellipses 'jackknifing' upon itself, allowing ellipses to overlap significantly. Since we wish to fit this model directly to the ECT-derived sinogram, we require an expression for the Radon transform of the dynamic ellipse model. The sinogram, as a function of projection direction $\theta(t)$, radial coordinate s and time t is given by

$$\begin{aligned} (\mathbf{R}E)(\theta(t), s, t, \mathbf{x}) &= \sum_{n=1}^N I_n(t) \times \\ &2 a_n b_n (a_n^2 \cos(\theta(t) + \Omega_n) + b_n^2 \sin(\theta(t) + \Omega_n))^{-1} \times \\ &\sqrt{(a_n^2 \cos(\theta + \Omega_n) + b_n^2 \sin(\theta + \Omega_n) - \\ &(s - u_n \cos(\theta) - v_n \sin(\theta))^2)}, \end{aligned} \quad (4)$$

where \mathbf{R} represents the Radon transform operator applied to the complete distribution $E(\mathbf{x})$

$$E(\mathbf{x}) = \sum_{n=1}^N E_n(\mathbf{x}_n), \quad \mathbf{x} = (\mathbf{x}_1, \mathbf{x}_2, \dots, \mathbf{x}_N). \quad (5)$$

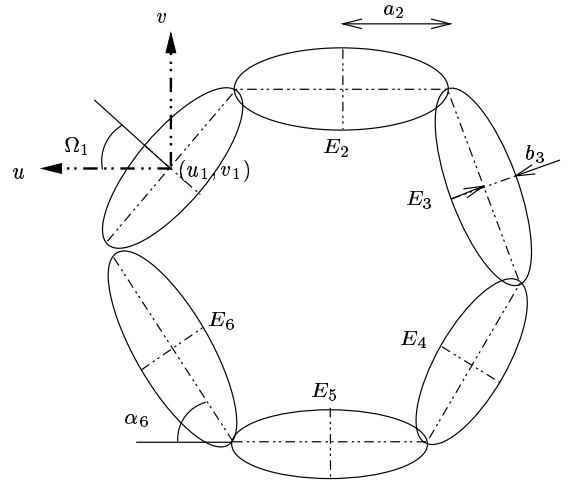


Figure 2: Typical elliptical region model

Physiological considerations provide us with bounds on both the geometric and kinetic parameters. For application to myocardial studies, we further constrain the spatial model to

force the constituent ellipses into a contiguous ring closed by E_N . These constraints, and further details relating to the model may be found in [1].

B. Inversion problem

A global-local hybrid optimization algorithm, which imposes physiologically motivated interval constraints on all parameters, is used to solve the least-squares problem:

$$\min_{\mathbf{x}} \sum_{p=0}^{P-1} \sum_{q=0}^{Q-1} \left[S(\theta(t_p), s_q, t_p) - (\mathbf{R}E)(\theta(t_p), s_q, t_p, \mathbf{x}) \right]^2, \quad (6)$$

where S is the acquired sinogram, containing P projections taken at time $t = t_p$ of Q bins each. The centers of the discrete bins are determined by the s_q values.

Even though the imposition of bounds on the values of the kinetic parameters restricts the number of possible solutions, we ideally desire a unique solution. This is not, in general, possible as the sums of the responses of several single compartment systems (convolved exponential sums) are not uniquely parameterized in the presence of noise [3, 4]. By finding an orthogonal basis set which, when convolved with the blood input function, is able to accurately represent all TAC's consistent with the underlying physiology in a study, we may find a 'more unique' description of each TAC. We find that optimizing for the coefficients of this convolved orthogonal basis, rather than a basis of decaying exponentials as in [5] greatly improves the condition of the problem, reduces the problem dimension and facilitates optimization of the objective function.

Employing M orthogonal basis functions $u_m[l]$, where $l = 0, 1, \dots, L-1$; is a discrete time index, the dynamic projections are given as

$$\begin{aligned} (\mathbf{R}E)(\theta(l\Delta t), s, l\Delta t, \mathbf{x}) &= i(t) * \sum_{n=1}^N \sum_{m=1}^M \mu^{mn} u_m[l] \times \\ &2 a_n b_n (a_n^2 \cos(\theta(l\Delta t) + \Omega_n) + b_n^2 \sin(\theta(l\Delta t) + \Omega_n))^{-1} \times \\ &\sqrt{(a_n^2 \cos(\theta(l\Delta t) + \Omega_n) + b_n^2 \sin(\theta(l\Delta t) + \Omega_n) - \\ &(s - u_n \cos(\theta(l\Delta t)) - v_n \sin(\theta(l\Delta t))))^2), \end{aligned} \quad (7)$$

and the parameter vector

$$\mathbf{x} = (a_1, b_1, \alpha_1, \mu^{11}, \dots, \mu^{M1}, u_1, v_1, \dots, a_N, b_N, \alpha_N, \mu^{1N}, \dots, \mu^{MN}, u_N, v_N), \quad (8)$$

replaces the parameterization in terms of the compartmental parameters given in (3).

III. MYOCARDIAL PHANTOMS

Figure 3 illustrates three ring configurations of ellipses which constitute perfect realizations of the geometric model used by the algorithm. These configurations, from the left to the right of the figure, consist of 5, 8 and 11 segments respectively. Since we expect fewer than 11 distinct dynamic

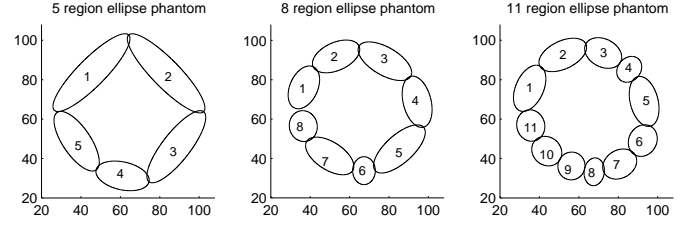


Figure 3: Closed ring elliptical model ideal realizations.

regions to be present within the myocardium, this number of shapes is chosen as the maximum number tested.

For greater realism, we generate our projection data not from model, as has been done in Figure 3, but from the three analogous segmented annular phantoms which appear in Figure 4.

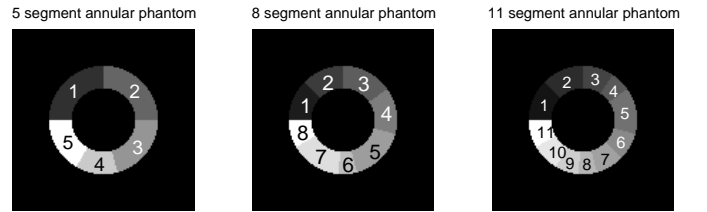


Figure 4: Annular phantoms used to generate simulated projection data.

Sinograms generated from these phantoms are realizations of Poisson processes with varying numbers of total counts. We evaluate the algorithm over a wide range of detected count values, from noise free conditions to as low as 1,000 detected events.

IV. PERFORMANCE METRICS

Conventionally, when compartmental models are fit to kinetic data, it is the accuracy with which the kinetic parameters are recovered that is used as metric of the performance of the estimation algorithm. However, when the compartmental model contains redundant parameters, as in the present case, different sets of parameter values may produce model responses whose differences may not be discernible in the presence of noise. Consequently, we feel that the true test of the viability of a kinetic parameter estimation algorithm is its ability to accurately recover the regional TAC's of dynamic imaged distribution. We therefore propose the metric:

$$M_{\text{pow}} \triangleq \frac{1}{N} \sum_{n=1}^N \frac{\sum_{l=0}^{L-1} (\phi_n[l] - \hat{\phi}_n[l])^2}{\sum_{l=0}^{L-1} \phi_n[l]^2} \times 100 \quad (9)$$

where $\phi_n[l]$ and $\hat{\phi}_n[l]$ are the true and recovered TAC's for region n , respectively.

V. EXPERIMENTAL RESULTS

The first three experiments evaluated algorithm TAC recovery in the absence of noise for the 5, 8 and 11 region cases. The algorithm was then applied to 10 Poisson sinogram realizations of each phantom at each of the count levels

1×10^6 , 2.5×10^5 , 1×10^5 , 1×10^4 and 1×10^3 detected events.

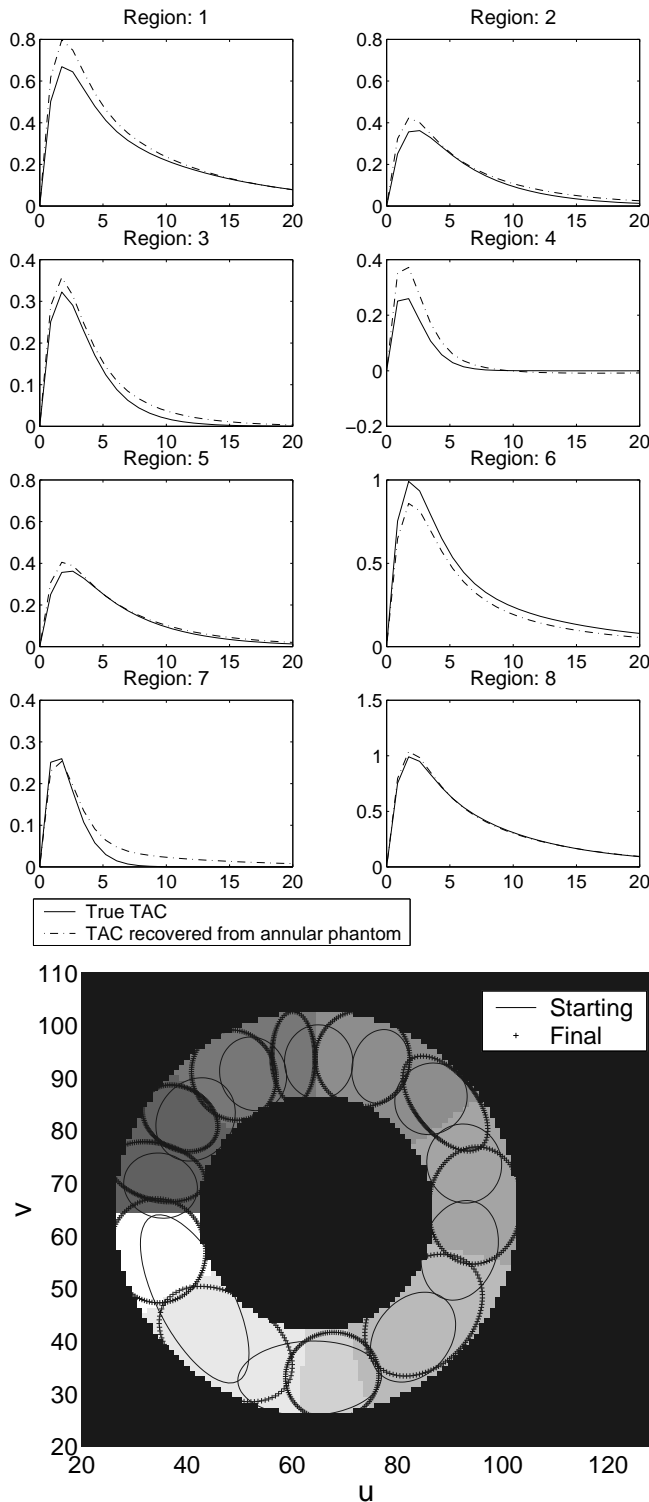


Figure 5: Typical spatiokinetic algorithm performance. Upper: True and recovered TAC's for each region. See Figure 4 for region number references. Lower: Initial ellipse placements before optimization are shown (solid) versus optimized positions (+). This simulation was performed at 1×10^6 detected counts.

Figure 6 illustrates algorithm performance versus the number of dynamic regions in the distribution, in terms of the metric M_{pow} . Error bars are shown spanning the mean \pm one standard deviation, and are staggered about the abscissa values of 5, 8 and 11 for legibility. For convenience, the same data are plotted with total detected counts as the abscissa in Figure 7.

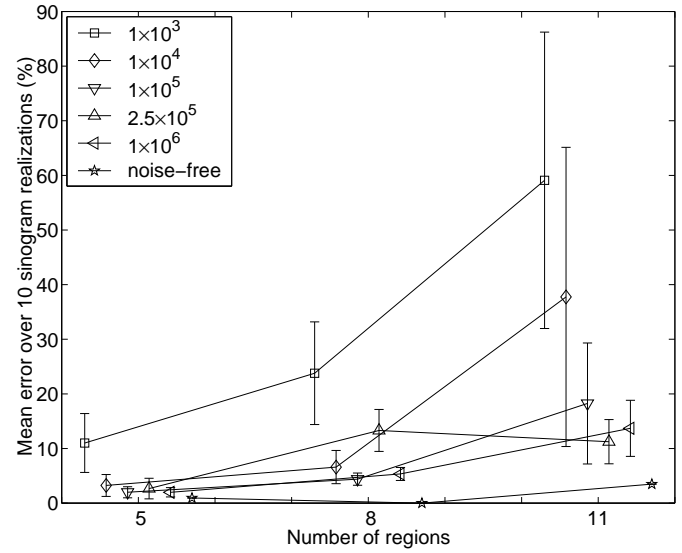


Figure 6: Error metric M_{pow} versus number of dynamic regions within distribution.

From consideration of Figures 6 and 7, it becomes apparent that a decrease in the SNR over the range in question is far more deleterious to the TAC estimates than an increase in the number of regions from 5 to 11. We make the following additional observations:

1. The increase in the TAC recovery error as the number of regions is increased, is only significant in the 11 shape case at the very poorest SNR's of 1×10^3 and 1×10^4 detected counts. Thus, in $^{99\text{m}}\text{Tc}$ -teboroxime clinical myocardial studies, where more than around 30,000 counts typically originate from the myocardium, it should be possible to resolve all regions sufficient in size to be of physiological significance in a functional sense. This assumes, however, that additional regions are defined so as to sufficiently model non-myocardial activity.
2. In the evaluation of most reconstruction algorithms, we expect the algorithm to produce estimates with very low error in the noise-free case. Here, we find that performance in the absence of noise is by no means perfect. This is indicative of just how poorly conditioned the optimization problem (6) is. The surface of the objective function contains so many local minima that a global search algorithm must be used to generate multiple start points for subsequent deterministic optimization. In all tests presented here, the generation of between 5 and 10 million initial parameter states was required before the solution stabilized.

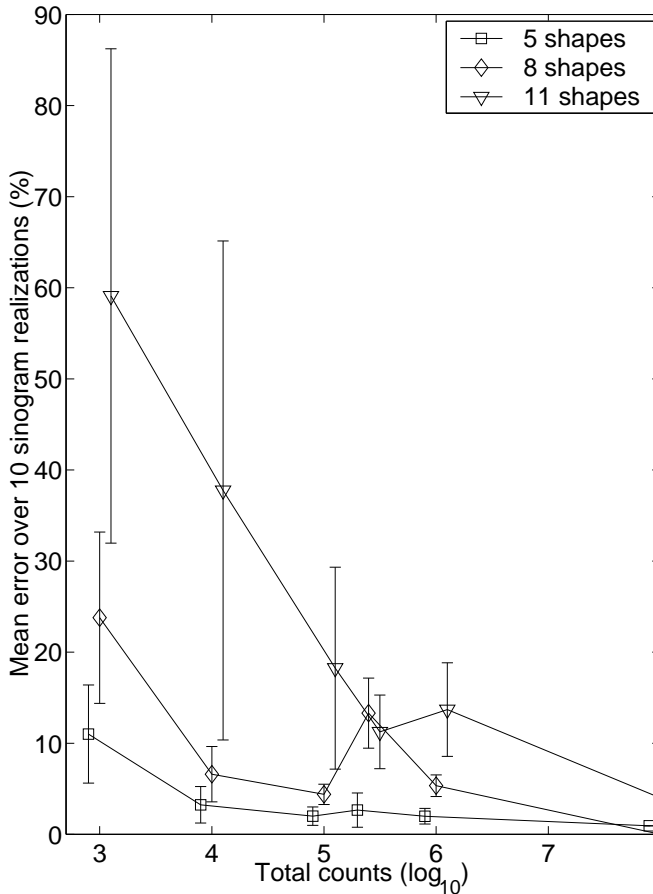


Figure 7: Error metric M_{pow} versus number of total detected sinogram counts.

The mean computation time for the execution of a single simulation study was 25.7 hours (Pentium II 400MHz).

VI. DISCUSSION

Our experimental results suggest that neither noise (at realistic levels) nor the number of regions (up to the maximum of 11 dynamic regions) included in the phantom significantly degrade the results of joint spatiokinetic estimation. Rather, the intrinsic difficulty in extricating individual regions and their time activities directly from projections limits estimation accuracy. As a result of this ill-conditioning, TAC's and region boundaries cannot, in general, be recovered exactly (in a finite amount of time), even when the estimation is performed under noise-free conditions. This is true even when the parameterized dynamic ellipses are fit to an elliptical ring phantom which is an exact realization of the model. Figure 8 illustrates such a failure to find the global minimum in a noise-free case, where a ring of 11 ellipses is fit to the 11 ellipse ideal model realization shown in Figure 3.

Our results suggest that multiregion joint spatial and kinetic reconstruction is feasible for obtaining kinetic estimates and dynamic region segmentations to within a useful degree of accuracy. The effects of realistic imaging conditions need to be established before these results can be translated into

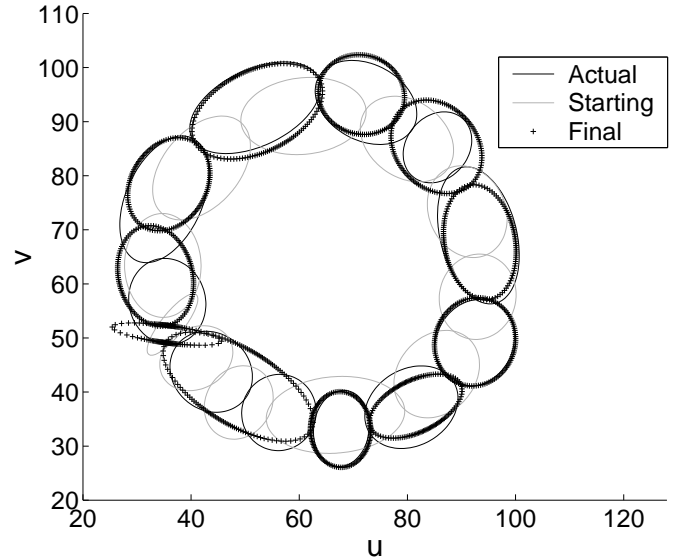


Figure 8: Even when the model is fit to a sinogram which is the set of projections of an exact realization of the model, under noise-free conditions, the global minimum may not be encountered. In this 11 region case, regions 9 and 10 are merged giving a sub-optimal solution. The algorithm is unable to find the global minimum even after 10 million invocations of the local optimization algorithm from stochastically generated starting points in the parameter space. This failure is due to the poor condition of the objective function surface.

practical feasibility guidelines. Future work should concentrate on the development of constrained geometric models for other functional anatomic structures so that spatiokinetic modeling of the entire field-of-view may be effected in dynamic ECT.

VII. ACKNOWLEDGEMENTS

I would like to thank Dr. Thomas F. Budinger and Dr. Elijah Polak for their invaluable contributions towards the development of the joint spatiokinetic reconstruction algorithm which was employed to obtain the results presented here.

VIII. REFERENCES

- [1] J. S. Maltz, E. Polak, and T. F. Budinger, "Multistart optimization algorithm for joint spatial and kinetic parameter estimation from dynamic ECT projection data," in *IEEE Nuclear Science Symposium and Medical Imaging Conference Record*, vol. 3, pp. 1567–1573, 1998.
- [2] P. C. Chiao, W. L. Rogers, N. H. Clinthorne, J. A. Fessler, and A. O. Hero, "Model-based estimation dynamic cardiac studies using ECT," *IEEE Transactions on Medical Imaging*, vol. 13, pp. 217–226, June 1994.
- [3] C. Lanczos, *Applied analysis*. Prentice-Hall, 1956.
- [4] J. G. Reich, "On parameter redundancy in curve fitting of kinetic data," in *Kinetic data analysis: design and analysis of enzyme and pharmacokinetic experiments* (L. Endrenyi, ed.), ch. IV, pp. 39–60, Plenum Press, 1981.
- [5] V. J. Cunningham and T. Jones, "Spectral analysis of dynamic PET studies," *Journal of Cerebral Blood Flow and Metabolism*, vol. 13, pp. 15–23, 1993.

- [6] A. M. Smith, G. T. Gullberg, P. E. Christian, and F. L. Datz, "Kinetic modeling of teboroxime using dynamic SPECT imaging of a canine model," *Journal of Nuclear Imaging*, vol. 35, pp. 484–495, Mar. 1994.
- [7] B. W. Reutter, G. T. Gullberg, and R. H. Huesman, "Kinetic parameter estimation from attenuated SPECT projection measurements," *IEEE Transactions on Nuclear Science*, vol. 45, no. 6, pp. 3007–3013, 1998.
- [8] B. W. Reutter, G. T. Gullberg, and R. H. Huesman, "Kinetic parameter estimation from dynamic cardiac patient SPECT projection measurements," in *1998 IEEE Nuclear Science Symposium and Medical Imaging Conference Record*, pp. 1953–1958, 1999.